

# CrystEngComm

Accepted Manuscript



This is an *Accepted Manuscript*, which has been through the Royal Society of Chemistry peer review process and has been accepted for publication.

*Accepted Manuscripts* are published online shortly after acceptance, before technical editing, formatting and proof reading. Using this free service, authors can make their results available to the community, in citable form, before we publish the edited article. We will replace this *Accepted Manuscript* with the edited and formatted *Advance Article* as soon as it is available.

You can find more information about *Accepted Manuscripts* in the [Information for Authors](#).

Please note that technical editing may introduce minor changes to the text and/or graphics, which may alter content. The journal's standard [Terms & Conditions](#) and the [Ethical guidelines](#) still apply. In no event shall the Royal Society of Chemistry be held responsible for any errors or omissions in this *Accepted Manuscript* or any consequences arising from the use of any information it contains.

## ARTICLE TYPE

# A Family of three magnetic metal organic frameworks: their synthesis, structural, magnetic and vapour adsorption study<sup>#</sup>

Suresh Sanda, Soumyabrata Goswami, Himanshu Sekhar Jena, Srinivasulu Parshamoni and Sanjit Konar\*

5 Received (in XXX, XXX) Xth XXXXXXXXXX 20XX, Accepted Xth XXXXXXXXXX 20XX

DOI: 10.1039/b000000x

Three flexible Metal-Organic Frameworks (MOFs) based on aldrithiol linker and pyromellitate ligand, namely, [Co(aldrithiol)(pyromellitate)<sub>0.5</sub>(H<sub>2</sub>O)<sub>2</sub>]<sub>n</sub> (**1**), [Ni<sub>2</sub>(aldrithiol)<sub>2</sub>(pyromellitate)(H<sub>2</sub>O)<sub>2</sub>]<sub>n</sub>·2n (C<sub>2</sub>H<sub>5</sub>OH)·11n H<sub>2</sub>O (**2**) and [Cu(aldrithiol)<sub>2</sub>(pyromellitate)]<sub>n</sub>·2n (H<sub>2</sub>O) (**3**) have been synthesized through  
10 slow diffusion technique and characterized by structural, magnetic and adsorption studies. Single crystal X-ray studies show that the compounds **1** and **3** have two-dimensional layered structures, whereas, compound **2** adopts a three-dimensional framework structure. The observed dimensionality change might be due to the different orientation of pyridine rings in flexible aldrithiol linker and versatile bridging modes of pyromellitate ligand. In **1** and **2**, pyromellitate ligand coordinates to the metal centre in  
15 monodentate fashion {(κ<sup>1</sup>)-(κ<sup>1</sup>)-(κ<sup>1</sup>)-(κ<sup>1</sup>)-μ<sub>4</sub>} and in **3**, it coordinates in {(κ<sup>1</sup>)-(κ<sup>1</sup>)-μ<sub>2</sub>} fashion. The magnetic properties of **1-3** were investigated in detail which shows weak antiferromagnetic coupling among the metal centres. Vapour sorption studies reveal that compound **1** and **3** show high methanol vapour uptake, whereas, compound **2** shows decent amount of H<sub>2</sub>O adsorption. The dehydrated frameworks of **1-3** regenerate the as-synthesized framework structure upon exposure to the water vapour.

## 20 Introduction

Metal-Organic-Frameworks (MOFs) have received extensive interest in the past few decades owing to their virtually endless number of possible structures with variable interesting structure related properties.<sup>1</sup> MOFs are also known for their potential  
25 applications in gas storage and separation,<sup>2</sup> catalysis,<sup>3</sup> drug delivery,<sup>4</sup> luminescence<sup>5</sup> and molecular magnetism<sup>6</sup> and other properties.<sup>7</sup> Literature reports reveal that MOFs containing only carboxylate ligands are fairly rigid<sup>8</sup> and the introduction of different pyridyl linkers along with carboxylate ligands introduce  
30 structural flexibility in the framework.<sup>9</sup> In this context, it is worthy to mention that the flexible MOFs have attracted considerable attention due to their dynamic behaviour such as single crystal to single crystal transformation,<sup>10</sup> unusual gas adsorption behaviour (stepwise, selective and sometimes  
35 hysteretic)<sup>11</sup> and guest responsive structural transformation.<sup>12</sup> etc. Usage of highly flexible organic linkers and carboxylates having wide variety of bridging modes in combination with magnetically potent transition metals result flexible frameworks with short metal-metal distance which is an important criteria for magnetic  
40 exchange.<sup>13</sup> Hence the resulted materials can be used as porous magnets or Magnetic Metal Organic Frameworks (MMOFs) which is a forefront research area.

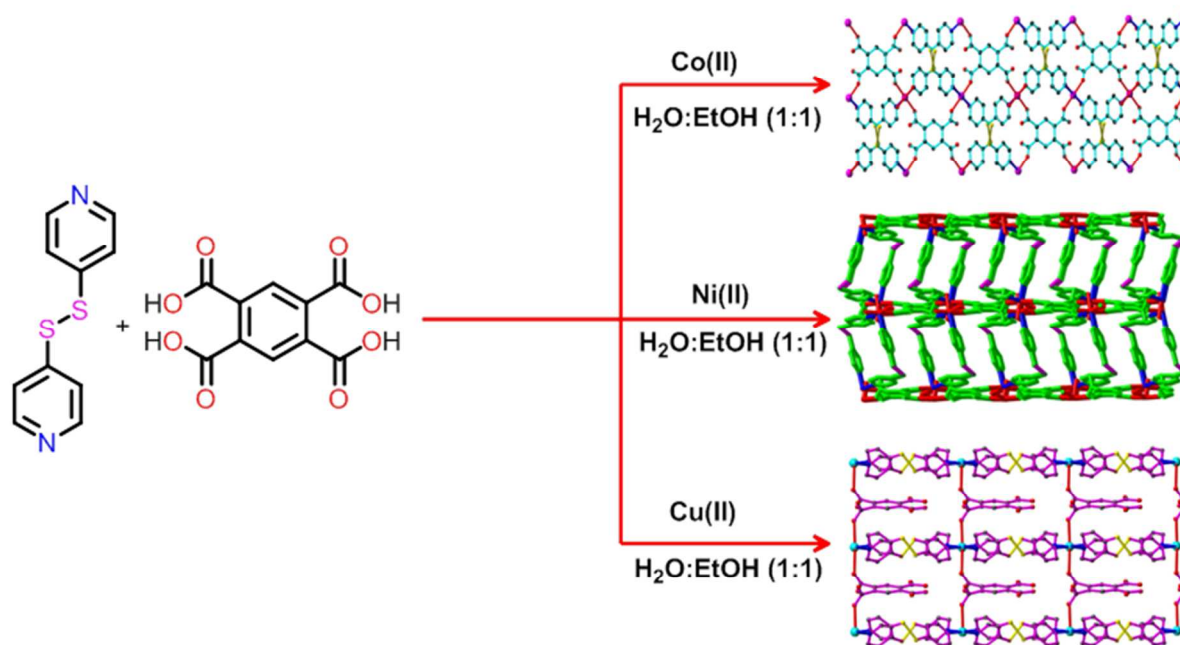
Recently, we have reported a third-generation breathing MOF of Zn(II) using flexible aldrithiol linker and pyromellitate ligand  
45 which shows selective, stepwise, reversible, and hysteretic adsorption properties.<sup>14</sup> We have extended our effort for other

transition metal ions like Co(II), Cu(II) and Ni(II) and herein we report two 2D MOFs and one 3D MOF having molecular formula [Co(aldrithiol)(pyromellitate)<sub>0.5</sub>(H<sub>2</sub>O)<sub>2</sub>]<sub>n</sub> (**1**),  
50 [Ni<sub>2</sub>(aldrithiol)<sub>2</sub>(pyromellitate)(H<sub>2</sub>O)<sub>2</sub>]<sub>n</sub>·2n (C<sub>2</sub>H<sub>5</sub>OH)·11n H<sub>2</sub>O (**2**) and [Cu(aldrithiol)<sub>2</sub>(pyromellitate)]<sub>n</sub>·2n (H<sub>2</sub>O) (**3**). The vapor adsorption and magnetic properties study of compounds reveal that they show bi-functional behaviour.

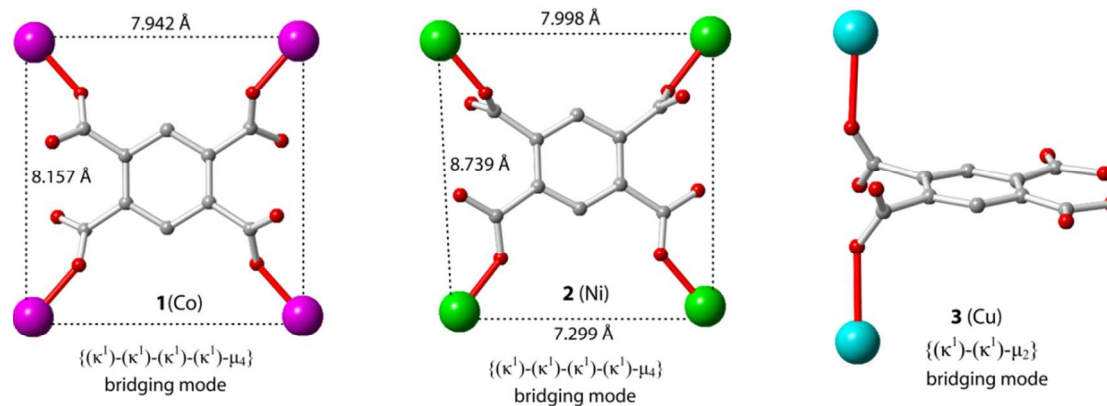
## Results and Discussions

### 55 Synthetic aspects

Aldrithiol (4,4'-dipyridyldisulfide) is one of the most flexible ligands which can be used to synthesize flexible MOFs. However, there are less number of reports available in the literature on flexible MOFs using aldrithiol as organic linker<sup>15</sup>  
60 and also there is no such report describing the gas and vapour adsorption properties except one.<sup>14</sup> In this regard, herein we report three flexible MOFs using aldrithiol linker, pyromellitate ligand and different metal ions like Co(II) (**1**), Ni(II) (**2**) and Cu(II) (**3**) in 1:0.25:1 ratio. The synthetic details are illustrated in  
65 Scheme 1. Compounds **1-3** are synthesized using Co(NO<sub>3</sub>)<sub>2</sub>·6H<sub>2</sub>O, Ni(ClO<sub>4</sub>)<sub>2</sub>·6H<sub>2</sub>O and Cu(NO<sub>3</sub>)<sub>2</sub>·2.5H<sub>2</sub>O respectively as metal source. Attempts to synthesize compound **2** by using Ni(NO<sub>3</sub>)<sub>2</sub>·6H<sub>2</sub>O results same structure. Compound **1-3** are synthesized at neutral pH conditions. It is worthy to note that  
70 although the same diffusion technique was followed to prepare all the three compounds (**1-3**), compounds **1** and **3** exhibits 2D framework whereas compound **2** reveals 3D framework structure.

**Scheme 1** Synthetic details for compounds 1-3.**Chart 1** Various bridging modes of pyromellitate ligand (a) and orientation of pyridine groups in the flexible aldrithiol linker (b) found in compounds 1-3.

(a) Various bridging modes of pyromellitate ligand.



(b) Orientation of pyridine groups in the flexible aldrithiol linker.

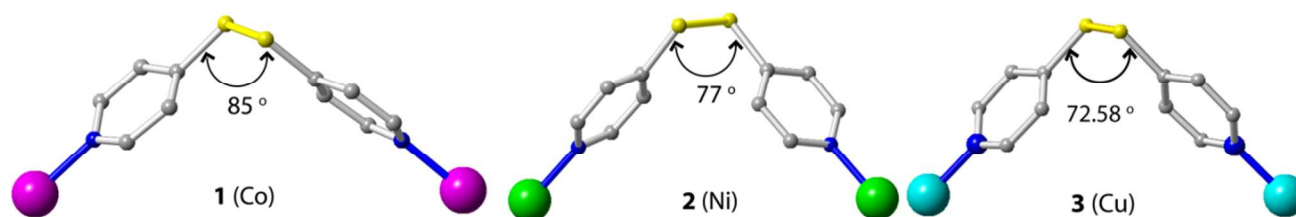


**Table 1** Crystallographic Data Parameters for Compounds 1-3.

	1	2	3
Empirical formula	C <sub>15</sub> H <sub>13</sub> N <sub>2</sub> O <sub>6</sub> S <sub>2</sub> Co	C <sub>34</sub> H <sub>52</sub> N <sub>4</sub> O <sub>25</sub> S <sub>4</sub> Ni <sub>2</sub>	C <sub>30</sub> H <sub>22</sub> N <sub>4</sub> O <sub>10</sub> S <sub>4</sub> Cu
CCDC number	973648	973650	973649
Formula weight	440.33	1162.43	790.32
Color	Pink	Green	Blue
Size (mm)	0.40 x 0.34 x 0.26	0.42 x 0.34 x 0.29	0.42 x 0.38 x 0.28
Crystal system	Orthorhombic	Monoclinic	Monoclinic
Space group	F d d d	C 2/c	P 2/c
a /Å	15.7239(19)	15.8979(12)	8.315(2)
b /Å	16.158(2)	15.7892(12)	10.205(3)
c /Å	40.866(10)	20.3288(16)	20.279(5)
α (°)	90.0	90.00	90.0
β (°)	90.0	106.324(8)	113.120(12)
γ (°)	90.0	90.00	90.00
Cell volume V(Å <sup>3</sup> )	10383(3)	4897.1(7)	1582.6(7)
Cell formula units Z	16	4	2
Wave length (Å)	0.71073	0.71073	0.71073
Temperature (K)	296(2)	296(2)	296(2)
Theta range for data collection	2.34 to 27.50	1.86 to 25.68	2.00 to 27.45
Total reflections	2990	2187	3617
Unique reflections	2987	1878	3564
F(000)	3552	2280	798
R <sub>factor</sub> all	0.0848	0.1013	0.0582
wR <sub>2</sub>	0.2475	0.2606	0.1713
Goodness-of-fit	1.117	1.162	1.009
(Δρ) <sub>max</sub> , (Δρ) <sub>min</sub> (e Å <sup>-3</sup> )	0.465, -0.874	0.420, -0.616	0.334, -0.771

The observed dimensionality change might be due to the versatile bridging modes of pyromellitate ligand (Chart 1(a)) and the flexibility of the aldrithiol linker (Chart 1(b)). The diffuse reflectance UV/Vis spectra of compounds 1-3 are displayed in Fig. S1 which shows different absorption features. The absorption of compounds 1-3 in UV region are observed at ~260 nm which corresponds to the intra-ligand n→π\* and π→π\* transition. In comparison with the free pyromellitate<sup>16a, b</sup> and aldrithiol<sup>16 c, d</sup> ligands, the absorptions in compounds 1-3 have been changed, suggesting that coordination of the metal ions alters the intrinsic electronic properties of the ligands. The absorptions of compounds 1-3 in the visible region are observed at 493 nm for 1, 635, 738 nm for 2, and 609 nm for 3 respectively which are due to the spin allowed d-d transition. It has been noticed that, the absorption intensities of compounds 2 and 3 are markedly higher than that of the compound 1 which attribute to the different bridging modes of both the ligands to the metal centre.

### Structural Description of compound 1

Compound 1 crystallizes in the orthorhombic system with space group Fddd. The asymmetric unit contains a Co(II) centre, half of pyromellitate ligand, half of aldrithiol linker and a coordinated water molecule (Fig. S2). Each Co(II) centre possess distorted octahedral geometry and the coordination environment is furnished by two carboxylate oxygen atoms (O1, O1A) of two different pyromellitate ligands, two nitrogen atoms (N1, N1A) from two aldrithiol linker and two coordinated water molecules (O3, O3A) (Fig. 1). It has been observed that the coordinated oxygen atoms of two pyromellitate ligands, nitrogen atom of one aldrithiol linker and one water molecule are at the equatorial positions, whereas, nitrogen atom of another aldrithiol linker and water molecule are located in the axial positions respectively. So, around each Co(II) centre, the pyromellitate ligands are *trans* to

each other (O1-Co1-O1A = 178.7(1)°), whereas, both the aldrithiol linkers (N1-Co1-N1A = 96.2(1)°) and water molecules (O3-Co1-O3A = 89.3(2)°) are *cis* to each other (Fig. 2).

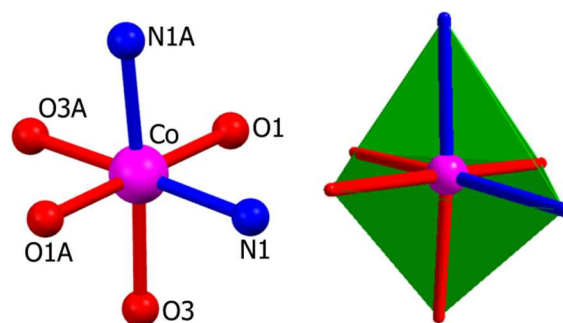


**Fig. 1.** Octahedral co-ordination environment around Co(II) centre in compound 1. Colour code: Cobalt (magenta), Nitrogen (blue), Oxygen (red).

The Co-O and Co-N bond lengths are in the range of 2.030(3)-2.159(4) Å respectively. In 1, each pyromellitate ligands holds four Co(II) centres in a monodentate fashion  $\{(\kappa^1)-(\kappa^1)-(\kappa^1)-(\kappa^1)-\mu_4\}$  leaving the remaining oxygen atoms uncoordinated (Chart 1(a)). Joining those four Co(II) centres by imaginary lines consequence a rectangular unit of dimensions 7.942 x 8.157 Å<sup>2</sup> (Chart 1(a)). Furthermore, the uncoordinated oxygen atoms of each pyromellitate ligands are involved in strong hydrogen bonding interactions (O(2)···O(3) = 2.586(7) Å) with coordinated water molecules (Table S2). In 1, the two pyridine rings of each flexible aldrithiol linker, are nearly perpendicular (~85°) to each other having a torsional angle of (C3-S1-S1A-C3A = 94.2(3)°) (Chart 1(b)) and coordinated to two nearby Co(II) centres. The distance between two Co(II) centres bridged by aldrithiol linker is 11.27 Å. Each Co(II) centres bridged by aldrithiol linkers are extended either in *a* or *b*- direction (Fig. 3) to form two

independent 1D chains. It is worthy to mention that those independent chains are stitched by pyromellitate ligands to form a 2D sheet in *ab*-plane (Fig. 4).

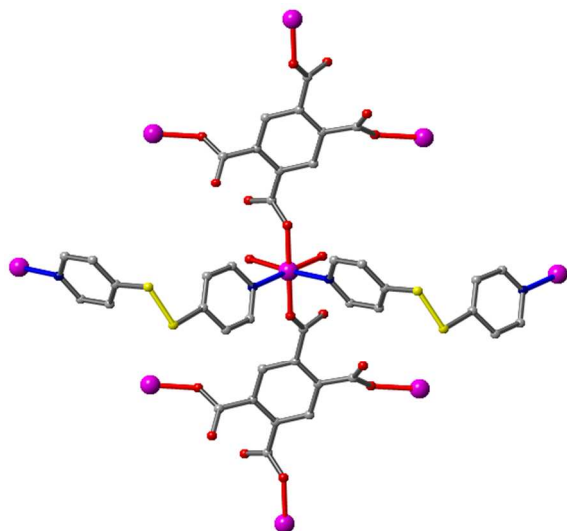


**Fig. 2.** Ball stick model showing the arrangement of pyromellitate ligands, aldrithiol linkers and coordinated water molecules around Co(II) centre found in **1**; colour codes, Co (magenta), O (red), N (blue), S (yellow) and C (grey).

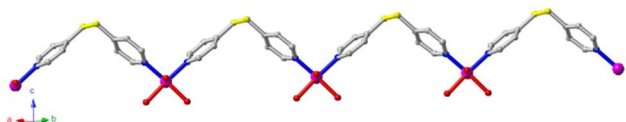


**Fig. 3.** 1D chain of compound **1** along the *b*-axis. Colour code: same as in Fig. 2.

Careful analysis reveals that each aldrithiol bridged 1D chains are crisscrossed over one another i.e. arranged on top and bottom of the plane containing pyromellitate ligands and Co(II) centres as shown in Fig. 5. Hence each aldrithiol linker occupies axial position at one Co(II) centre and equatorial position at another Co(II) centre in a particular 1D chain and creates a rectangular shaped voids along the *c*-direction as shown in Fig. 5. The rectangular voids are partially filled by the pyromellitate ligands. PLATON analysis reveals ~39% pore accessible void volume (4033.4 Å<sup>3</sup> per unit cell volume of 10383.0 Å<sup>3</sup>) in **1**. It can be seen that a basic unit, [Co(pyromellitate)<sub>2</sub>(aldrihtiol)<sub>2</sub>(OH<sub>2</sub>)<sub>2</sub>] is repeated to form complete 2D sheet and hence can be termed as Secondary Building Unit (SBU). Each SBUs are connected to six neighbouring SBUs by pyromellitate ligand and two SBUs by aldrithiol linkers to form the extended structure.

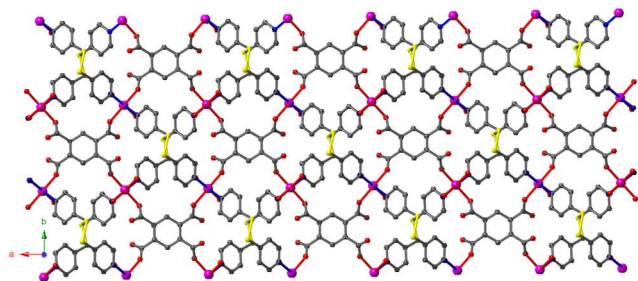


**Fig. 4.** Illustration of 2D sheet found compound **1**. Colour code: same as in Fig. 2.

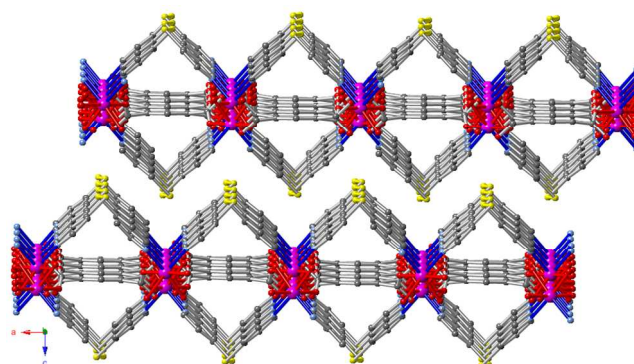


**Fig. 5.** Illustration of extended rectangular voids and the arrangement of pyromellitate ligands inside it found in **1**. Colour code: same as in Fig. 2.

### Structural Description of compound **2**

Compound **2** crystallizes in monoclinic crystal system with space group C2/c. The asymmetric unit consists of one Ni(II) centre, half of a pyromellitate ligand, one aldrithiol linker, six guest water molecules and one ethanol molecule respectively (Fig. S3). each Ni(II) centre is hexa coordinated and bridged by two nitrogen atoms (N1 and N2) from two aldrithiol linkers, two oxygen atoms (O2 and O3) from two pyromellitate ligands and two coordinated water molecules (O5 and O6) creating a distorted octahedral geometry (Fig. S4). Similar to **1**, in **2**, two pyromellitate ligands, one aldrithiol linker and one coordinated water molecule are at the equatorial positions and the remaining aldrithiol linkers, coordinated water molecule are in axial site. The pyromellitate ligands are located *trans* to each other (O2-Ni1-O3 = 178.8(4) °), whereas, aldrithiol linkers (N1-Ni1-N2 = 94.9(5) ° and the position of coordinated water molecules (O5-Ni1-O6 = 87.0(4) °) are *cis* to each other (Fig. 6). The Ni-O and Ni-N bond lengths are in range of 2.029(9)-2.123(9) Å respectively.

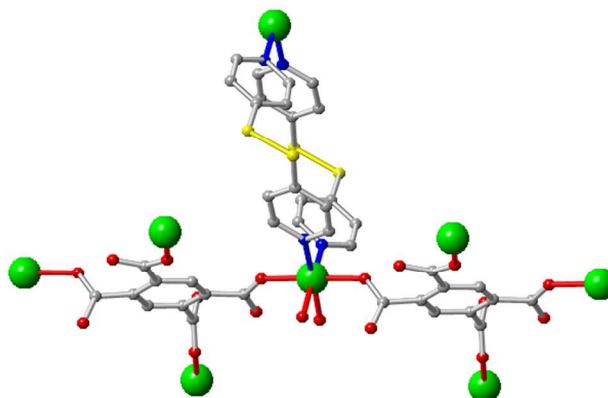


**Fig. 6.** Ball stick model showing the arrangement of pyromellitate ligands, aldrithiol linkers and coordinated water molecules around Ni(II) centre found in **2**. colour codes, Ni (Green), O (red), N (blue), S (yellow) and C (grey).

Similar to **1**, in **2** each pyromellitate ligands holds four Ni(II) centres in a monodentate fashion  $\{(\kappa^1)-(\kappa^1)-(\kappa^1)-(\kappa^1)-\mu_4\}$  leaving the remaining oxygen atoms uncoordinated (Chart 1(a)) and extended in the *ab*-plane to form a 2D layered structure. Joining those four Ni(II) centres by imaginary lines consequence a distorted molecular rectangle. The Ni $\cdots$ Ni distances in the rectangles are 7.299(3), 7.998(2) and 8.739(3) Å respectively

(Chart 1(a)). The above distortion is due to the flexible arrangement of carboxy groups of pyromellitate ligands. On comparing the orientation of carboxy groups of pyromellitate ligand in **1** and **2**, it is very interesting to note that in **1**, each carboxy groups are orientated at an angle of  $\sim 45^\circ$  whereas in **2** two carboxy groups are orientated at an angle of  $\sim 12^\circ$  and other two are at  $\sim 83^\circ$  to the mean plane containing phenyl ring of pyromellitate ligand (Chart 1(a)). Thus, the different arrangements of carboxy groups of pyromellitate ligands enforce two Ni(II) centres in the same plane containing phenyl ring of pyromellitate ligand and other two Ni(II) centres at a distance of 1.386 Å on the above and below of that plane. The uncoordinated oxygen atoms of the pyromellitate ligand are involved in strong hydrogen bonding interaction ( $O1-O6 = 2.640(1)$  and  $O4-O5 = 2.680(1)$  Å) with coordinated water molecules as well as solvated water molecules respectively (Table S2). In **2**, the two pyridine rings of aldrithiol linker are subtended at an angle of  $77^\circ$  to each other having a torsional angle of ( $C3-S1-S2-C6 = 75.9(7)^\circ$ ) and coordinates to two nearby Ni(II) centres in a "V" shape manner and forms centrosymmetric dimer (Fig. S5). The distance between two Ni(II) centres in the dimer is 9.917(2) Å. The nearby centrosymmetric dimers are stabilized by a  $\pi \cdots \pi$  interaction of 3.592 Å ( $cg \cdots cg$ ) between pyridine rings of two adjacent aldrithiol linkers. Each Ni(II) dimers are further connected perpendicularly to the afore mentioned 2D layer and extended it to form a 3D framework structure (Fig. 7). In the 3D framework one basic unit  $[Ni(pyromellitate)_2(aldrithiol)_2(OH_2)_2]$  is repeated to form the complete framework and hence can be termed as Secondary Building Unit (SBU). Each SBUs are connected to one nearby SBU through aldrithiol bridge and six SBUs through pyromellitate ligands. 3D framework houses two types of extended channels (A and B); channel A is formed by the  $[Ni_2(aldrithiol)_2]$  centrosymmetric dimers and channel B by  $[Ni_4(aldrithiol)_4(pyromellitate)_2]$  (Fig. 7). It is interesting to note that those channels are arranged alternatively and are hydrophilic in nature i.e. they are filled by the solvent water and ethanol molecules. PLATON analysis reveals no solvent accessible area in the 3D framework. However, the desolvated framework contains  $\sim 39\%$  pore accessible void volume ( $1904.7 \text{ \AA}^3$  per unit cell volume  $4897.1 \text{ \AA}^3$ ).

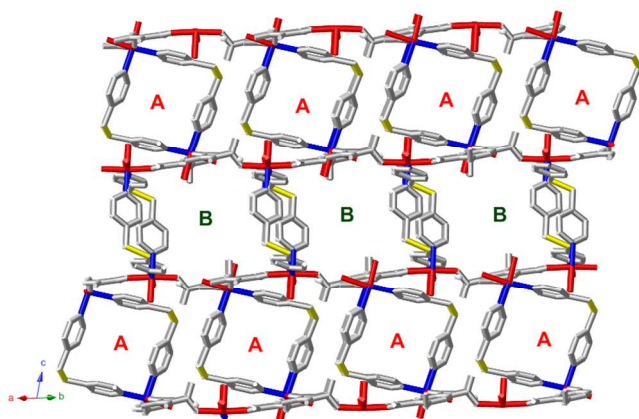


Fig. 7. Illustration of 3D framework with channels (A and B) found in compound **2**. Colour codes same as in Fig. 6.

The solvent molecules inside each channel are stabilized by hydrogen bonding interaction between themselves and also with the uncoordinated oxygen atoms of the pyromellitate ligands (Fig. S6). The hydrogen bond parameters are listed in Table S2.

### Structural description of compound **3**

Compound **3** crystallizes in monoclinic system with P2/c space group. The asymmetric unit of **3** consists one Cu(II) centre, half of a pyromellitate ligand, one aldrithiol linker and one solvated water molecule respectively (Fig. S7). Each Cu(II) centre is hexacoordinated and bridged by four nitrogen atoms from four different aldrithiol linkers (N1, N1A, N2, N2A) and two oxygen atoms from two different pyromellitate ligands (O4, O4A) forming a distorted octahedral geometry (Fig. 8). It is important to note that in compound **1** and **2**, two coordinated water molecules are present whereas in **3**, they are absent and their positions are now occupied by two more aldrithiol linkers. In **1** and **2** the pyromellitate ligands are sited in equatorial positions and aldrithiol linkers in both equatorial and axial positions, whereas, in **3** all the equatorial positions are occupied by aldrithiol linkers ( $N3-Cu1-N3A = 91.6(1)^\circ$  and  $N4-Cu1-N4A = 92.2(1)^\circ$ ) and the axial positions by pyromellitate ligands ( $O4-Cu1-O4A = 177.0(1)^\circ$ ) (Fig. 9). The Cu-N and Cu-O bond lengths are in range of 2.020(3)–2.542(4) Å respectively. It is key to note that the observed longer Cu-O bond length in **3** in comparison to **1** and **2** due to the smaller size of Cu(II) in comparison to Co(II) and Ni(II).

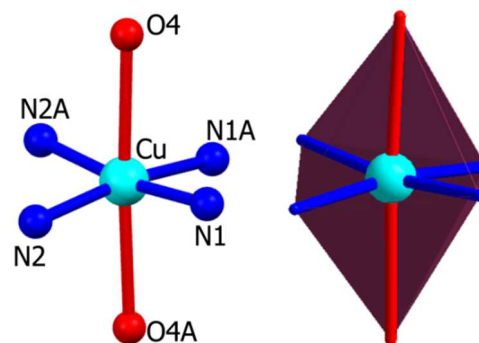


Fig. 8. Octahedral coordination environment around Cu(II) centre in compound **3**.

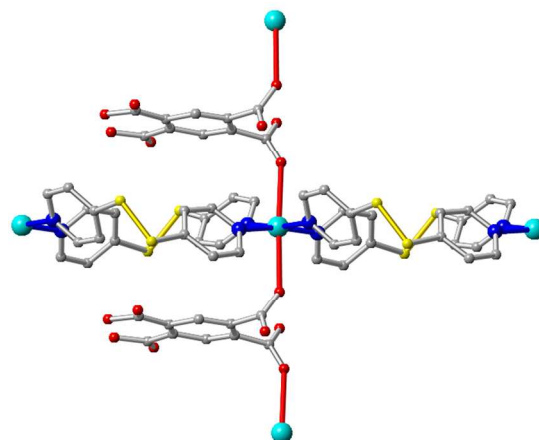
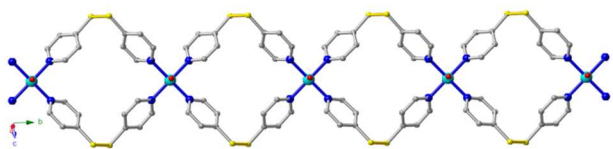
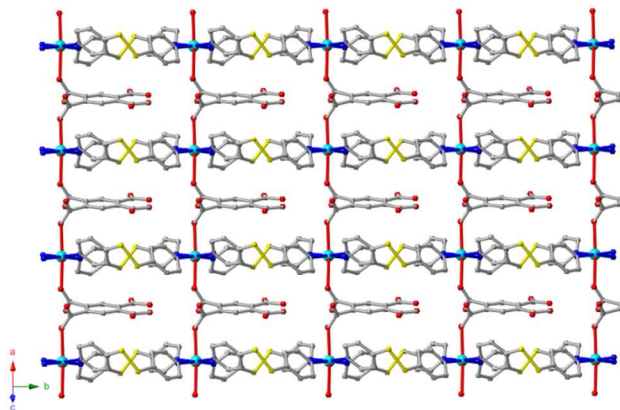


Fig. 9. Ball stick model showing the arrangement of pyromellitate ligands and aldrithiol linkers around Cu(II) centre found in **3**. colour codes, Cu (cyan), O (red), N (blue), S (yellow) and C (grey).

The observed longer Cu-O bond length in **3** in comparison to **1** and **2** due to the smaller size of Cu(II) in comparison to Co(II) and Ni(II). Compare to to compound **1** and **2**, in **3** only two carboxy group of pyromellitate ligand coordinates to two Cu(II) centres in monodentate bridging mode  $\{(\kappa^1)-(\kappa^1)-\mu_2\}$  and the remaining oxygen atoms from two other carboxy groups do not participate in coordination (Chart 1(a)). The distance between two Cu(II) centres bridged by single pyromellitate ligand is 8.315(2) Å. Such bridging mode pyromellitate ligands extend the dimer units to form a 1D chain along the *a*-direction. The uncoordinated oxygen atoms of two carboxy groups are strongly H-bonded to each other (O2-O2A = 2.362(6) Å) H-bonded to each other. Besides, the oxygen atoms of uncoordinated carboxy groups are stabilized by various C-H...O interactions (3.239(6) - 3.473(6) Å) with the aldrithiol linkers. In **3**, two pyridine ligands of the flexible aldrithiol linkers are oriented at an angle of  $\sim 72.58^\circ$  and subtend a torsional angle of  $82.5^\circ$  (C7-S1-S2-C3) between them. Similar to compound **2**, in **3**, each aldrithiol linker bridged to two different Cu(II) centres at a distance of 10.205(3) Å to form a centrosymmetric dimer. Each dimer further extended through aldrithiol linker to form 1D chain along the *b*-direction (Fig. 10). These 1D chains are further extended by the pyromellitate ligands along the *a*-direction to form a 2D layer in the *ab*-plane (Fig. 11).



**Fig. 10** 1D chain of compound **3** along the *b*-axis. Colour codes same as in Fig. 9.



**Fig. 11** Illustration of 2D framework showing the arrangements of pyromellitate ligands and aldrithiol linkers found in compound **3**. Colour codes same as in Fig. 9.

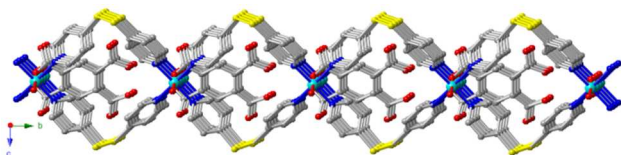


**Fig. 12** Illustration of 2D framework showing the arrangements of pyromellitate ligands on the above and below of channels found in compound **3**. Colour codes same as in Fig. 9.

It is very interesting to note that in the aforementioned 2D layer, the pyromellitate ligands are sandwiched between the two nearby

aldrithiol bridged 1D chains and located at above and below the channels (Fig. 11). This peculiar arrangement of the pyromellitate ligands restrict the opening of channels (Fig. 12). PLATON analysis reveals no solvent accessible area in the 2D layer. However the desolvated framework contains only  $\sim 9\%$  pore accessible void volume ( $135.5 \text{ \AA}^3$  per unit cell volume  $1582.6 \text{ \AA}^3$ ). The arrangements of pyromellitate ligands in the channels are favoured by the weak C-H... $\pi$  (3.470(6) Å) and C-H...O interactions (3.239(6)- 3.473(6) Å) respectively. Further the aforementioned 2D layers are interlinked through hydrogen bonding interaction (O3...O5 = 2.671(5) Å; O5...O5 = 2.726(4) Å) with the solvated water molecules residing in the 2D interlayer space to form a 3D framework (Fig. S8). It can be seen that, one basic unit  $[\text{Cu}(\text{pyromellitate})_2(\text{aldrithiol})_4]$  is repeated to form the complete framework and hence termed as Secondary Building Unit (SBU). Each SBUs are connected to two nearby SBU through aldrithiol bridge and two SBUs by pyromellitate ligands.

### Thermal and PXRD Analysis

To check the thermal stability of compounds **1-3**, thermo gravimetric analysis (TGA) was carried out in the temperature range of 30 - 500 °C under a flow of  $\text{N}_2$  with a heating rate of  $10.^\circ\text{C min}^{-1}$  (Fig. S9). Compound **1** shows a weight loss of  $\sim 8\%$  (Calcd.  $\sim 9\%$ ) in the temperature range of 93 - 145 °C which corresponds to the weight loss of two coordinated water molecules from the framework. In **2**, weight loss of  $\sim 23\%$  (Calcd.  $\sim 25\%$ ) was observed in the temperature range of 40 - 154 °C which corresponds to the loss of eleven solvated water and one ethanol molecules from the framework and the desolvated framework is stable up to 230 °C. Similarly compound **3** shows a weight loss of  $\sim 5\%$  (calcd.  $\sim 5\%$ ) in the temperature range of 36 - 105 °C, which corresponds to the loss of two solvated  $\text{H}_2\text{O}$  molecules from the framework. The powder XRD (PXRD) analyses of compounds **1-3** (Fig. S10-S12) are in very good correspondence with their corresponding simulated patterns obtained from the single crystal, indicating the phase purity of bulk samples.

### Magnetic studies

#### Magnetic properties of compound **1**

A variable temperature magnetic susceptibility data of a powder sample of **1** was measured at 0.1T as shown in Fig. 13. At 300 K, a  $\chi_M T$  ( $\chi_M$  = molar magnetic susceptibility) value of  $2.56 \text{ cm}^3 \text{ mol}^{-1} \text{ K}$  is obtained with an effective magnetic moment ( $\mu_{\text{eff}}$ ) of  $4.54 \mu_B$  per formula unit, which is higher than the spin-only value of  $3.87 \mu_B$  for a high spin Co(II) ion. This might be due to the orbital contribution typical for the  $^4\text{T}_{1g}$  ground state of octahedral high-spin Co(II) ion.<sup>17</sup> The  $1/\chi_M$  data for complex **1**, within the temperature range of 1.8 - 300 K, were fitted to the Curie-Weiss equation,  $[\chi_M = C/(T-\theta)]$ , which afforded the Curie constant,  $C = 2.62 \text{ cm}^3 \text{ mol}^{-1} \text{ K}$ , and Weiss constant,  $\theta = -11.39 \text{ K}$  (Fig. S13 inset), indicating an antiferromagnetic exchange interaction between the Co(II) centres. The  $\chi_M T$  plot shows a continuous decline to a minimum value of  $1.39 \text{ cm}^3 \text{ mol}^{-1} \text{ K}$  at 1.8 K. Further, on lowering the temperature, both the FC and ZFC susceptibilities gradually increase following each other and the value of  $\chi_M$  at 1.8 K is about  $0.77 \text{ cm}^3 \text{ mol}^{-1}$ , showing no phase transition (Fig. S13). Thus, the temperature-dependency of both

$\chi_M$  and  $\chi_M T$  are in accordance with the antiferromagnetic behaviour in **1**. The isothermal magnetization curve ( $M/N\mu_B$  vs.  $H$  plot, Fig. 13 inset) shows a saturation value of 1.79  $N\mu_B$  per formula unit at 2 K and 7 T, which is lower than the saturation value of 3  $N\mu_B$  for spin-only Co(II) ion ( $S = 3/2$  and  $g = 2$ ).<sup>18</sup> This behaviour also supports an antiferromagnetic coupling between the Co(II) ions in **1**.

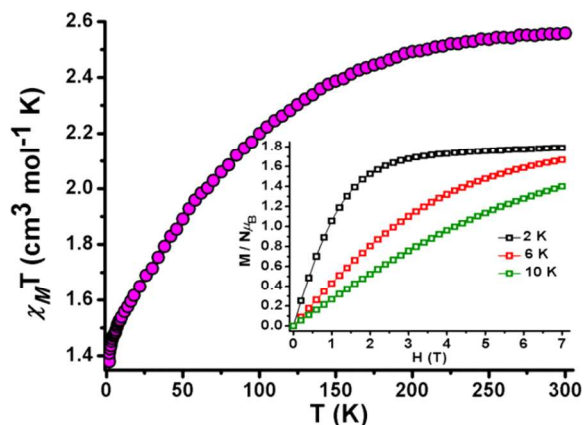


Fig. 13.  $\chi_M T$  vs  $T$  curve measured at 0.1 T for complex **1**. The inset curve presents field dependence of magnetization of **1** at 2, 6 and 10 K.

#### Magnetic properties of compound **2**

A variable-temperature magnetic susceptibility data was collected for **2** at an applied dc field of 0.01 T in the temperature range of 1.8 - 300 K as shown in Fig. 14. At around 300 K, the value of  $\chi_M T$  is 1.25  $\text{cm}^3 \text{mol}^{-1} \text{K}$  with a  $\mu_{\text{eff}}$  of 3.17  $\mu_B$  per formula unit, which is slightly higher than the spin-only value of 2.83  $\mu_B$  for a Ni(II) ion. As the temperature is lowered from 300 K,  $\chi_M T$  value shows small decrease up to about 1.01  $\text{cm}^3 \text{mol}^{-1} \text{K}$  at 15 K as expected for isolated Ni(II) ions with  $S = 1$ . This is in agreement with the lack of suitable magnetic exchange pathways between the metal centres because of appreciable metal-metal distance (7.3 - 11.2 Å). Below 15 K,  $\chi_M T$  decreases sharply and reaches a value of 0.72  $\text{cm}^3 \text{mol}^{-1} \text{K}$  at 1.8 K.

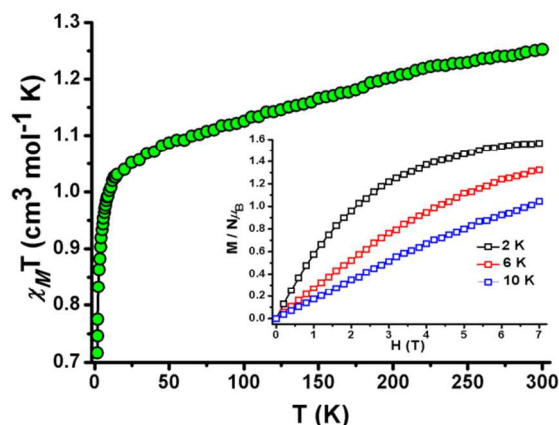


Fig. 14.  $\chi_M T$  vs  $T$  curve measured at 0.01 T for complex **2**. The inset curve presents field dependence of magnetization of **2** at 2, 6 and 10 K.

The inverse susceptibility data ( $1/\chi_M$ ) obeys the Curie-Weiss law with  $C = 1.24 \text{ cm}^3 \text{mol}^{-1} \text{K}$  and  $\theta = -5.08 \text{ K}$  (Fig. S14 inset), indicating very weak antiferromagnetic exchange interaction between the Ni(II) centres. In case of **2** also the FC and ZFC susceptibility data increase with temperature following each other

and the  $\chi_M$  value at 1.8 K is about 0.39  $\text{cm}^3 \text{mol}^{-1}$ , showing no phase transition (Fig. S14). The  $M/N\mu_B$  vs  $H$  curve measured at 2 K displays no hysteresis loop (Fig. S15) and variable field magnetization measurements at 2 K and 7 T shows a saturation value of 1.56  $N\mu_B$  per formula unit (Fig. 14 inset), which is slightly lower than the saturation value of 2  $N\mu_B$  for spin-only Ni(II) ion ( $S = 1$  and  $g = 2$ ).

#### Magnetic properties of compound **3**

A variable-temperature dc magnetic susceptibility data has also been obtained for complex **3** at 0.01 T in the temperature range of 1.8 - 300 K and is shown in Fig. 15 in the form of  $\chi_M T$  vs  $T$ . At room temperature, a  $\chi_M T$  value of 0.36  $\text{cm}^3 \text{mol}^{-1} \text{K}$  and a  $\mu_{\text{eff}}$  of 1.70  $\mu_B$  is observed and upon cooling, the susceptibility value remains nearly constant up to  $\sim 20 \text{ K}$  wherefrom the value decreases more rapidly to  $\sim 0.26 \text{ cm}^3 \text{mol}^{-1} \text{K}$  down to the lowest temperature of 1.8 K. Fit of the magnetic data was done by using the Curie - Weiss law which afforded  $C = 0.36 \text{ cm}^3 \text{mol}^{-1} \text{K}$  and  $\theta = -1.53 \text{ K}$  (Fig S16 inset). The slow decrease in  $\chi_M T$  and effective magnetic moment in high temperature region and the low negative  $\theta$  indicates weak antiferromagnetic coupling between Cu(II) sites, which is due to the long Cu(II)  $\cdots$  Cu(II) distance in the range of 8.3 - 13.1 Å. The FC and ZFC susceptibility data increase with temperature following each other and the  $\chi_M$  value at 1.8 K is about 0.14  $\text{cm}^3 \text{mol}^{-1}$ , showing no phase transition (Fig. S16). Variable field magnetization measurements (Fig. 15 inset) show that the reduced magnetization value rises fairly rapidly and begins to plateau at higher magnetic fields reaching a saturation value of 0.85  $N\mu_B$  per formula unit at 2 K and 7 T.

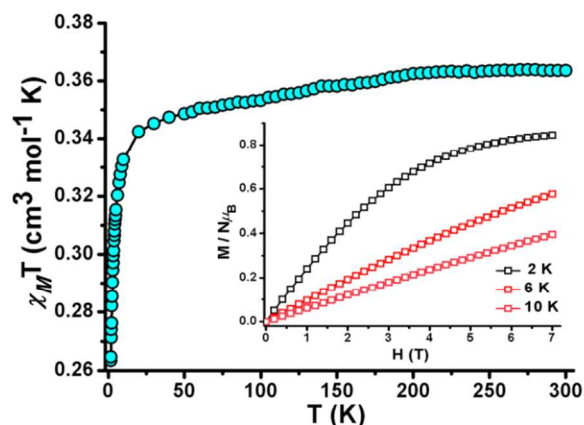


Fig. 15.  $\chi_M T$  vs  $T$  curve measured at 0.01 T for complex **3**. The inset curve presents field dependence of magnetization of **3** at 2, 6 and 10 K.

#### Adsorption properties

To explore the porous properties of compounds **1-3** adsorption measurements were carried out with gases like  $\text{N}_2$ ,  $\text{CO}_2$  and  $\text{H}_2$  (Fig. S17-S20). Adsorption isotherms of  $\text{N}_2$  at 77 K and  $\text{CO}_2$  at 195 K and 298 K show very less uptake whereas no uptake was observed with  $\text{H}_2$  at 77 K in all three compounds.

To understand the interaction of host frameworks with solvent molecules, we carried out vapour adsorption measurements with different polar solvents. Sorption Isotherm with  $\text{H}_2\text{O}$  shows 80  $\text{mL g}^{-1}$ , 161  $\text{mL g}^{-1}$  and 124  $\text{mL g}^{-1}$  of uptake in compounds **1**, **2** and **3** respectively (Fig. 16). Compared to **1** and **3**, large volume

of H<sub>2</sub>O adsorption in the case of **2** is expected as in the crystal structure of compound **2**, there are large numbers of guest water molecules present in the pores. In **1** and **3** the carboxylate oxygen atoms of the pyromellitate ligands pointed towards the middle portion of 1D channel which might also causes the decrease in adsorption amount.

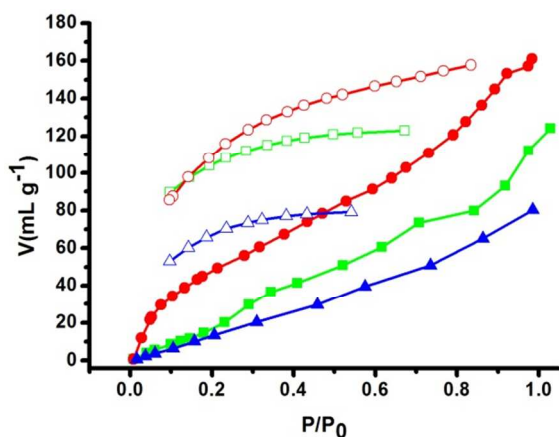


Fig. 16. H<sub>2</sub>O adsorption isotherms of compounds 1-3. **1**(blue), **2**(red) and **3** (green).

The incomplete desorption in compounds **1** and **3** is might be due to the hydrogen bonding interaction between the free carboxylate oxygen atoms and adsorbed H<sub>2</sub>O molecules and for **2** it is due to the re-accumulation of H<sub>2</sub>O molecules in pores. The PXRD patterns after complete H<sub>2</sub>O vapour adsorbed samples of compounds **1-3** (Fig. S21-23) are similar to that of the as-synthesized compounds which further supports that compounds **1-3** achieved its original structure as a result of re-accumulation of H<sub>2</sub>O molecules inside the pores and coordination sites. Interestingly, encouraging results were obtained in the MeOH/CH<sub>3</sub>CN sorption profiles of **1** and **3**. In comparison to H<sub>2</sub>O adsorption, the uptake amounts were increased in compounds **1** and **3** whereas the adsorption amount was drastically decreased in the case of **2**. The adsorption profile with MeOH in **1** and **3** shows 155 mL g<sup>-1</sup> and 195 mL g<sup>-1</sup> with two-step isotherm whereas less uptake (67 mL g<sup>-1</sup>) was obtained for compound **2** with no steps in isotherm (Fig. 17). Similar sorption profiles were obtained in the case of CH<sub>3</sub>CN with less adsorption amounts compare to MeOH (Fig. 18). The less adsorption amount and different sorption profile of compound **2** in comparison to **1** and **3** suggest that some additional adsorption sites are available for MeOH/CH<sub>3</sub>CN in compounds **1** and **3**. From the crystal structures of **1** and **3** it can be observed that the hydrophobic benzene moieties of pyromellitate ligands were exposed to the middle of the pores (Fig. 5 and 12). As MeOH/CH<sub>3</sub>CN molecules containing both hydrophilic -OH/CN as well as hydrophobic -CH<sub>3</sub> parts they could strongly interact with the hydrophobic benzene rings of pyromellitate ligands which enhances the MeOH/CH<sub>3</sub>CN uptake in **1** and **3**.<sup>19</sup> The first step adsorption is might be due to pore filling and the second step could be ascribed by the strong interaction with the hydrophobic channel surface through the methyl group.<sup>19b</sup> The less adsorption amount in case of CH<sub>3</sub>CN can be justified by correlating the large molecular diameter (4.3 Å) and less polarity of CH<sub>3</sub>CN compared to MeOH.<sup>20</sup>

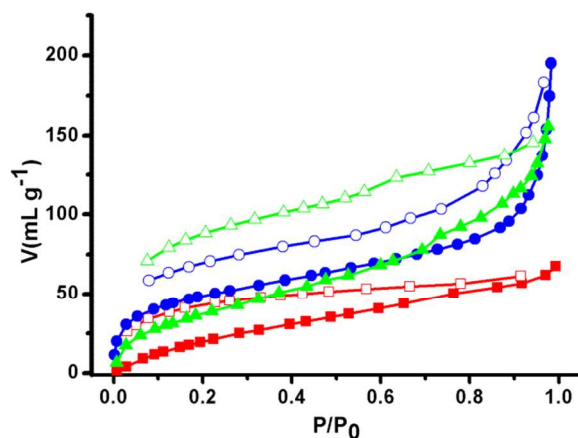


Fig. 17. MeOH adsorption isotherms of compounds 1-3. **1**(blue), **2**(red) and **3**(green).

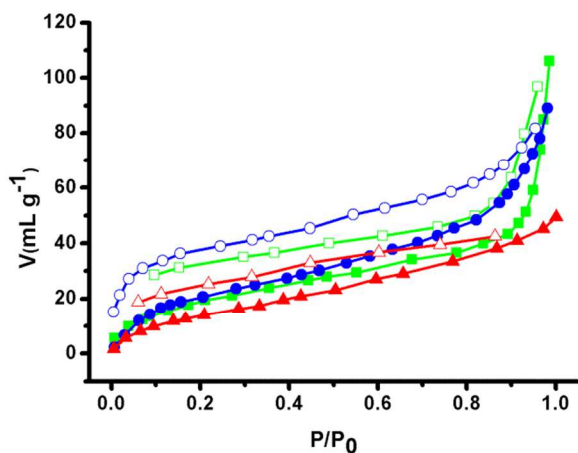


Fig. 18. Acetonitrile adsorption isotherms of compounds 1-3. **1**(blue), **2**(red) and **3**(green).

## Conclusions

We have successfully synthesized two 2D MOFs and one 3D MOF using mixed-ligand strategy along with three different paramagnetic transition metal ions. The change in structural dimensionality highlights the impact of the flexibility of aldrithiol linker and diverse bridging mode of pyromellitate ligands on the synthesis of flexible MOFs. Variable-temperature and variable-field magnetic moment measurements demonstrate that compounds **1-3** show weak antiferromagnetic interactions among the metal centres. Vapour adsorption studies reveal that compounds **1** and **3** show high methanol adsorption, whereas, compound **2** show considerable amount of H<sub>2</sub>O adsorption. The above findings conclude that suitable choice of ligand combination along with metal ions engender adsorption as well as magnetic or other properties in the resulting materials and make them multi-functional in nature. Further work in this direction is underway.

## Experimental section

### General Information

All the metal salts and solvents were commercially available and were used as obtained. 1,2,4,5-Benzene tetracarboxylic acid (Pyromellitic acid) and Aldrithiol were obtained from the Sigma-

Aldrich Chemical Co. India.

### Physical measurements

Thermo gravimetric analysis was recorded on Perkin-Elmer TGA 4000 instrument. IR spectrum of the compounds **1-3** were recorded on Perkin-Elmer FT-IR Spectrum BX using the KBr pellets in the region 4000 - 400 cm<sup>-1</sup>. Elemental analysis was carried out on Elementar Micro vario Cube Elemental Analyzer. PXRD patterns were measured on PAnalytical EMPYRIAN instrument by using Cu K $\alpha$  radiation. Magnetic measurements were performed using a Quantum Design SQUID VSM magnetometer. The measured values were corrected for the experimentally measured contribution of the sample holder, while the derived susceptibilities were corrected for the diamagnetism of the samples, estimated from Pascal's tables.<sup>21</sup> Gas adsorption measurements were performed by using BelSorpmax (BEL Japan) automatic volumetric adsorption instrument. All the gases used were of Ultra-pure research grade (99.999%). HPLC grade solvents were used for vapour adsorption studies.

### Synthesis of [Co(aldriithiol)(pyromellitate)<sub>0.5</sub>(H<sub>2</sub>O)<sub>2</sub>]<sub>n</sub> (**1**):

An aqueous solution of (5 mL) sodium salt of pyromellitate (0.05 mmol, 17.1 mg) was added stepwise to the ethanol solution (5 mL) of aldriithiol (0.1 mmol, 22 mg) while being stirred and the resulting solution was further stirred for 1 hour more to mix well. Co(NO<sub>3</sub>)<sub>2</sub>·6H<sub>2</sub>O (0.1 mmol, 29.1 mg) was dissolved in 10 mL of water and kept in a narrow tube. 2 mL of the above mixed ligand solution was slowly and carefully layered over 2 mL of the metal solution and tube was kept undisturbed at room temperature. X-ray quality pink colored single crystals were obtained from the junction of the layer after 10 days. The crystals were separated and washed with ethanol and air-dried (yield = 43% based on cobalt). Elemental analysis: Anal. Calcd: C, 40.9%; H, 2.9%; N, 6.3%; S, 14.5%; Found: C, 40.1%; H, 2.4%; N, 5.8%; S, 13.9%; FT-IR (KBr pellet, cm<sup>-1</sup>): 3411(br), 3169(w), 1631(m), 1583(w), 1433(s), 1058(br).

### Synthesis of [Ni<sub>2</sub>(aldriithiol)<sub>2</sub>(pyromellitate)(H<sub>2</sub>O)<sub>2</sub>]<sub>n</sub> · 2n(C<sub>2</sub>H<sub>5</sub>OH)·11n(H<sub>2</sub>O) (**2**)

Compound **2** has been synthesized following the same diffusion technique applied for compound **1** using the Ni(ClO<sub>4</sub>)<sub>2</sub>·6H<sub>2</sub>O in place of Co(NO<sub>3</sub>)<sub>2</sub>·6H<sub>2</sub>O. X-ray quality green colored single crystals were obtained from the junction of the layer after 15 days. Yield (33% based on nickel). Elemental analysis. Anal. Calcd: C, 35.1%; H, 4.5%; N, 4.8%; S, 11.0%. Found: C, 34.5%; H, 4.1%; N, 4.1%; S, 10.5%. FT-IR (KBr pellet cm<sup>-1</sup>) 3440(br), 1590(s), 1480(w), 1401(s), 1324(w), 1213(m), 1102(br).

### Synthesis of [Cu(aldriithiol)<sub>2</sub>(pyromellitate)]<sub>n</sub>·2n(H<sub>2</sub>O) (**3**)

The same diffusion technique as followed for compound **1** was employed for the synthesis of compound **3** using Cu(NO<sub>3</sub>)<sub>2</sub>·2.5H<sub>2</sub>O in place of Co(NO<sub>3</sub>)<sub>2</sub>·6H<sub>2</sub>O. X-ray quality blue colored single crystals were obtained from the junction of the layer after 20 days. Yield (31% based on copper) Elemental analysis. Anal. Calcd: C, 45.5%; H, 2.8%; N, 7.0%; S, 16.2%. Found: C, 44.9%; H, 2.4%; N, 6.4%; S, 15.5%. FT-IR (KBr pellet cm<sup>-1</sup>) 3424(br), 1636(m), 1607(s), 1434(s), 1309(w), 1239(w), 1009(w).

### X-ray Crystallographic Analysis

Single crystal data for compounds **1-3** were collected on a Bruker SMART diffractometer equipped with a graphite monochromator and Mo-K $\alpha$  ( $\lambda = 0.71073 \text{ \AA}$ , 296 K) radiation. Data collection was performed using  $\phi$  and  $\omega$  scan. The structures were solved using direct methods followed by full matrix least square refinements against F<sup>2</sup> (all data HKLF 4 format) using SHELXTL.<sup>22</sup> Subsequent difference Fourier synthesis and least-square refinement revealed the positions of the remaining non-hydrogen atoms. Determinations of the crystal system, orientation matrix, and cell dimensions were performed according to the established procedures. Lorentz polarization and multi-scan absorption correction were applied. Non-hydrogen atoms were refined with independent anisotropic displacement parameters and hydrogen atoms were placed geometrically and refined using the riding model. All calculations were carried out using SHELXL 97,<sup>23</sup> PLATON 99,<sup>24</sup> and WinGXsystemVer-1.64.<sup>25</sup> As compound **1** contains solvent accessible void, SQUEEZE<sup>25</sup> programme was applied and details about the squeezed material from the .SQF file is included in the final .CIF file. For compounds **1-3**, the hydrogen atoms of the coordinated water molecules and solvent molecules were not located by riding methods, however are included in the molecular formula. Data collection and structure refinement parameters and crystallographic data for the compounds **1-3** are given in Table 1. Selected bond lengths and bond angles for compounds **1-3** are given in Table S1.

### Acknowledgements

SS, SG, SP thank IISER Bhopal for the PhD fellowships and HSJ thanks for post-doctoral fellowship. S.K. thanks CSIR, Government of India (Project No.01/(2473)/11/EMR II), and IISER Bhopal for generous financial and infrastructural support.

### Notes and references

# Dedicated to Professor N. Ray Chaudhuri on the occasion of his 72th Birthday

Department of Chemistry, IISER Bhopal, Bhopal 462023, MP, India.  
E-mail: skonar@iiserb.ac.in; Fax: +91-755-6692392; Tel: +91-755-6692339.

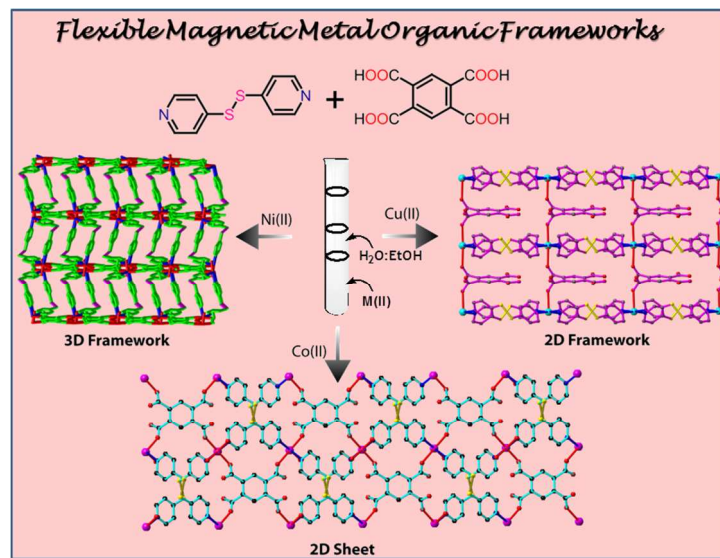
† Electronic Supplementary Information (ESI) available: PXRD, TGA and additional figures, magnetic and gas adsorption data. See DOI: 10.1039/b000000x.

- (a) S. Kitagawa, R. Kitaura and S. Noro, *Angew. Chem. Int. Ed.*, 2004, **43**, 2334; (b) C. Janiak, *J. Chem. Soc., Dalton Trans.*, 2003, 2781; (c) O. M. Yaghi, M. O'Keeffe, N. W. Ockwing, H. K. Chae, M. Eddaoudi, and J. Kim, *Nature.*, 2003, **423**, 705; (d) D. N. Dybtsev, M. P. Yutkin, E. V. Peresypkina, A. V. Virovets, C. Serre, G. Ferey and V. P. Fedin, *Inorg. Chem.*, 2007, **46**, 6843.
- (a) J. R. Li, J. Sculley and H. C. Zhou, *Chem. Rev.*, 2012, **112**, 869; (b) H. Furukawa, K. E. Cordova, M. O'Keeffe and O. M. Yaghi, *Science.*, 2013, **341**, 974; (c) L. J. Murray, M. Dinca and J. R. Long, *Chem. Soc. Rev.*, 2009, **38**, 1294; (d) W. Yang, A. J. Davies, X. Lin, M. Suyetin, R. Matsuda, A. J. Blake, C. Wilson, W. Lewis, J. E. Parker, C. C. Tang, M. W. George, P. Hubberstey, S. Kitagawa, H. Sakamoto, E. Bichoutskaia, N. R. Champness, S. Yang and M. Schroder, *Chem. Sci.*, 2012, **3**, 2993.
- (a) L. Ma, C. Abney and W. Lin, *Chem. Soc. Rev.*, 2009, **38**, 1248; (b) D. N. Dybtsev, A. L. Nuzhdin, H. Chun, K. P. Bryliakov, E. P. Talsi, V. P. Fedin and K. Kim, *Angew. Chem. Int. Ed.*, 2006, **45**, 916; (c) S. H. Cho, B. Ma, S. T. Nguyen, J. T. Hupp and T. E. Albrecht-Schmittb, *Chem. Commun.*, 2006, 2563.

- 4 (a) O. K. Farha and J. T. Hupp, *Acc. Chem. Res.*, 2010, **43**, 1166; (b) P. Horcajada, C. Serre, M. Vallet-Regi, M. Sebban, F. Taulelle and G. Férey, *Angew. Chem. Int. Ed.*, 2006, **45**, 5974; (c) J. D. Rocca, D. Liu and W. Lin, *Acc. Chem. Res.*, 2011, **44**, 957. and references cited there in.
- 5 (a) L. E. Kreno, K. Leong, O. K. Farha, M. Allendorf, R. P. Van Duyne and J. T. Hupp, *Chem. Rev.*, 2012, **112**, 1105. and references cited therein; (b) S. Sanda, S. Parshamoni, A. Adhikary and S. Konar, *Cryst. Growth Des.*, 2013, **13**, 5442. (c) Y. Cui, Y. Yue, G. Qian, and B. Chen, *Chem. Rev.*, 2012, **112**, 1126. and references cited therein.
- 10 6 (a) C. N. R. Rao, A. K. Cheetham and A. Thirumurugan, *J. Phys. Condens. Matter.*, 2008, **20**, 083202; (b) A. Chakraborty, B. K. Ghosh, J. B. Arino, J. Ribas and T. K. Maji, *Inorg. Chem.*, 2012, **51**, 6440; (c) G. J. Halder, C. J. Kepert, B. Moubaraki, K. S. Murray and J. D. Cashion, *Science*, 2002, **298**, 1762; (d) M. Kurmoo, *Chem. Soc. Rev.* 2009, **38**, 1353. and reference cited therein; (e) S. Goswami, S. Sanda and S. Konar, *CrystEngComm.*, 2014, **16**, 369; (f) C. Dey, R. Das, B. K. Saha, P. Poddar and R. Banerjee, *Chem. Commun.*, 2011, **47**, 11008; (g) S. Goswami, A. Adhikary, H. S. Jena, S. Biswas and S. Konar *Inorg. Chem.* 2013, **52**, 12064.
- 20 7 (a) C. Dey, T. Kundu and R. Banerjee, *Chem. Commun.*, 2012, **48**, 266; (b) T. Panda, T. Kundu and R. Banerjee, *Chem. Commun.*, 2012, **48**, 5464; (c) P. K. Thallapally, J. W. Grateb and R. K. Motkuri, *Chem. Commun.*, 2012, **48**, 347; (d) S. Jin, H.-J. Son, O. K. Farha, G. P. Wiederrecht and J. T. Hupp, *J. Am. Chem. Soc.*, 2013, **135**, 955.
- 25 8 (a) M. Eddaoudi, J. Kim, N. Rosi, D. Vodak, J. Wachter, M. O’Keeffe and O. M. Yaghi, *Science*, 2002, **295**, 469; (b) M. Eddaoudi, H. L. Li and O. M. Yaghi, *J. Am. Chem. Soc.*, 2000, **122**, 1391.
- 30 9 (a) J. Seo, R. Matsuda, H. Sakamoto, C. Bonneau and S. Kitagawa, *J. Am. Chem. Soc.*, 2009, **131**, 12792; (b) I. Beurroies, M. Boulhout, P. L. Llewellyn, B. Kuchta, G. Férey, C. Serre and R. Denoyel, *Angew. Chem. Int. Ed.*, 2010, **49**, 7526; (c) M. Dan-Hardi, H. Chevreau, T. Devic, P. Horcajada, G. Maurin, G. Férey, D. Popov, C. Riekel, S. Wuttke, J.-C. Lavalley, A. Vimont, T. Boudewijns, D. de Vos and C. Serre, *Chem. Mater.*, 2012, **24**, 2486; (d) P. K. Thallapally, J. Tian, M. Radha Kishan, C. A. Fernandez, S. J. Dalgarno, P. B. McGrail, J. E. Warren and Jerry L. Atwood, *J. Am. Chem. Soc.*, 2008, **130**, 16842.
- 40 10 (a) K. Biradha and M. Fujita, *Angew. Chem. Int. Ed.*, 2002, **41**, 3392; (b) S. Mohapatra, H. Sato, R. Matsuda, S. Kitagawa and T. K. Maji, *CrystEngComm.*, 2012, **14**, 4153; (c) T. K. Maji, G. Mostafa, R. Matsuda and S. Kitagawa, *J. Am. Chem. Soc.*, 2005, **127**, 17152.
- 45 11 (a) T. K. Kim and M. P. Suh, *Chem. Commun.*, 2011, **47**, 4258; (b) D. H. Hong and M. P. Suh, *Chem. Commun.*, 2012, **48**, 9168; (c) N. F. Sciortino, K. R. Scherl-Gruenwald, G. Chastanet, G. J. Halder, K. W. Chapman, J. F. Letard and C. J. Kepert, *Angew. Chem. Int. Ed.*, 2012, **51**, 10154; (d) J. Zhang, H. Wu, T. J. Emge and J. Li, *Chem. Commun.*, 2010, **46**, 9152.
- 50 12 (a) B. Manna, A. K. Chaudhari, B. Joarder, A. Karmakar and S. K. Ghosh, *Angew. Chem. Int. Ed.*, 2013, **52**, 998; (b) H. B. Cui, B. Zhou, L. -S. Long, Y. Okano, H. Kobayashi and A. Kobayashi, *Angew. Chem. Int. Ed.*, 2008, **47**, 3376; (c) J. A. R. Navarro, E. Barea, A. Rodriguez-Dieguez, J. M. Salas, C. O. Ania, J. B. Parra, N. Masciocchi, S. Galli and A. Sironi, *J. Am. Chem. Soc.*, 2008, **130**, 3978.
- 55 13 (a) B. K. Tripuramallu, S. Mukherjee and S. K. Das, *Cryst. Growth Des.*, 2012, **12**, 5579; (b) P. Manna, B. K. Tripuramallu and S. K. Das, *Cryst. Growth Des.*, 2012, **12**, 4607; (c) B. K. Tripuramallu, P. Manna, S. N. Reddy and S. K. Das, *Cryst. Growth Des.*, 2012, **12**, 777; (d) B. K. Tripuramallu and Samar K. Das, *Cryst. Growth Des.*, 2013, **13**, 2426; (e) B. K. Tripuramallu, R. Kishore and Samar K. Das *Polyhedron.*, 2010, **29**, 2985.
- 60 14 S. Sanda, S. Parshamoni and S. Konar, *Inorg. Chem.*, 2013, **52**, 12866.
- 65 15 (a) G. Marin, M. Andruh, A. M. Madalan, A. J. Blake, C. Wilson, N. R. Champness, and M. Schröder, *Cryst. Growth Des.*, 2008, **8**, 964; (b) J. P. Lang, Q. F. Xu, W.-H. Zhang, H.-X. Li, Z.-G. Ren, J.-X. Chen and Y. Zhang, *Inorg. Chem.*, 2006, **45**, 10487; (c) A. J. Blake, N. R. Brooks, N. R. Champness, M. Crew, A. Deveson, D. Fenske, D. H. Gregory, L. R. Hanton, P. Hubbersteya and Martin Schröder, *Chem. Commun.*, 2001, 1432; (d) R. Carballo, B. Covelo, N. F. Hermida, A. B. Lago and E. M. Vazquez-Lopez, *CrystEngComm.*, 2009, **11**, 817; (e) A. K. Ghosh, D. Ghoshal, J. Ribas, E. Zangrando, N. R. Chaudhuri, *J. Molecular Str.*, 2006, 796,195; (f) J. Luo, M. Hong, R. Wang, D. Yuan, R. Cao, L. Han, Y. Xu and Z. Lin, *Eur. J. Inorg. Chem.*, 2003, 3623.
- 70 16 (a) D. Chandra, M. W. Kasture and A. Bhaumik, *Micropor. Mesopor. Mater.*, 2008, **116**, 204; (b) S.V. Ganesan, P. Lightfoot and S. Natarajan, *Solid State Sci.*, 2004, **6**, 757; (c) J. Luo, M. Hong, R. Wang, D. Yuan, R. Cao, L. Han, Y. Xu and Z. Lin, *Eur. J. Inorg. Chem.*, 2003, 3623; (d) L. Han, X. Bu, Q. Zhang and P. Feng, *Inorg. Chem.*, 2006, **45**, 5736.
- 75 17 (a) V. Laget, C. Hornick, P. Rabu, M. Drillon and R. Ziessel, *Coord. Chem. Rev.*, 1998, **178-180**, 1533, and references cited therein; (b) B. N. Figgis, M. Gerloch, J. Lewis, F. E. Mabbs and G. A. Webb, *J. Chem. Soc. A*, 1968, 2086; (c) M. Gerloch and P. N. Quedsted, *J. Chem. Soc. A*, 1971, 3729; (d) F. E. Mabbs and D. J. Machin, *Magnetism in Transition Metal Complexes*, Chapman and Hall, London, 1973; (e) C. M. Nagaraja, N. Kumar, T. K. Maji and C. N. R. Rao, *Eur. J. Inorg. Chem.*, 2011, 2057; (f) S. Khatua, S. Goswami, S. Parshamoni, H. S. Jena and S. Konar, *RSC advances*, 2013, **3**, 25237.
- 80 18 X. Y. Wang, L. Gan, S. W. Zhang, S. Gao, *Inorg. Chem.*, 2004, **43**, 4615.
- 85 19 (a) P. Kanoo, K. L. Gurunatha and T. K. Maji, *J. Mater. Chem.*, 2010, **20**, 1322; (b) K. L. Gurunatha and T. K. Maji, *Inorg. Chem.*, 2009, **48**, 10886.
- 90 20 (a) T. K. Maji, S. Pal, K. L. Gurunatha, A. Govindaraj and C. N. R. Rao, *Dalton Trans.*, 2009, 4426; (b) S. Mohapatra, H. Sato, R. Matsuda, S. Kitagawa and T. K. Maji, *CrystEngComm.*, 2012, **14**, 4153; (c) S. K. Ghosh, R. Azhakar and S. Kitagawa, *Chem. Asian J.*, 2009, **4**, 870.
- 95 21 O. Kahn, *Molecular Magnetism*; VCH: New York, 1993.
- 100 22 G. M. Sheldrick, SHELXTL, *Program for the Solution of Crystal of Structures*; University of Goettingen: Goettingen, Germany, 1993.
- 105 23 G. M. Sheldrick, SHELXL 97, *Program for Crystal Structure Refinement*; University of Goettingen: Goettingen, Germany, 1997.
- 110 24 A. L. Spek, *J. Appl. Crystallogr.* 2003, **36**, 7.
- 115 25 L. J. Farrugia, *J. Appl. Crystallogr.* 1999, **32**, 837.

5

## Table of Contents



10

Three flexible Magnetic Metal-Organic Frameworks (MOFs) have been synthesized and their magnetic and adsorption properties were investigated.

15

20

25

30

35